Article:
Jemth, A.-S., Scaletti, E., Carter, M. et al. (2019) Crystal structure and substrate specificity of the 8-oxo-dGTP hydrolase NUDT1 from Arabidopsis thaliana. Biochemistry, 58 (7). pp. 887-899. ISSN: 0006-2960

https://doi.org/10.1021/acs.biochem.8b00950

Crystal structure and substrate specificity of the 8-oxo-dGTP hydrolase NUDT1 from *Arabidopsis thaliana*

Ann-Sofie Jemth[1], Emma Scaletti[2], Megan Carter[2], Thomas Helleday[1,3] and Pål Stenmark[2,4*]*

[1]Science for Life Laboratory, Division of Translational Medicine and Chemical Biology, Department of Medical Biochemistry and Biophysics, Karolinska Institutet, S-171 21 Stockholm, Sweden.

[2]Department of Biochemistry and Biophysics, Stockholm University, S-106 91 Stockholm, Sweden.

[3]Sheffield Cancer Centre, Department of Oncology and Metabolism, University of Sheffield, S10 2RX Sheffield, UK.

[4]Department of Experimental Medical Science, Lund University, Lund, Sweden.

KEYWORDS: *Arabidopsis thaliana,* 8-oxo-dGTP, Nudix enzymes, Nucleotide metabolism

ABSTRACT: *Arabidopsis thaliana* NUDT1 (AtNUDT1) belongs to the Nudix family of proteins, which have a diverse range of substrates, including oxidized nucleotides such as 8-oxo-dGTP.

The hydrolysis of oxidized dNTPs is highly important as it prevents their incorporation into DNA, thus preventing mutations and DNA damage. AtNUDT1 is the sole Nudix enzyme from *A. thaliana* shown to have activity against 8-oxo-dGTP. We present the structure of AtNUDT1 in complex with 8-oxo-dGTP. Structural comparison with bacterial and human homologues reveals a conserved overall fold. Analysis of the 8-oxo-dGTP binding mode shows that the residues Asn76 and Ser89 interact with the O8 atom of the substrate, a feature not observed in structures of protein homologs solved to date. Kinetic analysis of wild-type and mutant AtNUDT1 confirmed that these active site residues influence 8-oxo-dGTP hydrolysis. A recent study showed that AtNUDT1 is also able to hydrolyze terpene compounds. The diversity of reactions catalyzed by AtNUDT1 suggests that this Nudix enzyme from higher plants has evolved in a manner distinct to those from other organisms.

INTRODUCTION

Nudix (nucleoside diphosphates linked to some moiety x) proteins are a class of pyrophosphohydrolases characterized by the conserved amino acid sequence GX_5EX_7REVXEEXGU, where U is a hydrophobic residue.[1] These proteins are found in more than 250 species throughout eukaryotes, bacteria and archaea.[2] Nudix enzymes catalyze the hydrolysis of a wide variety of substrates including ribo- and deoxyribonucleoside triphosphates (and their oxidized forms), dinucleotide polyphosphates, nucleotide sugars, NADH, coenzyme A and ADP-ribose.[3-5] Nudix proteins are critical for regulating the concentrations of these compounds, which are either toxic, constitute metabolic intermediates or are important cell signaling molecules.[1] Most Nudix hydrolases require divalent cations such as Mg^{2+} or Mn^{2+} for full activity.[6] The Nudix motif conserved in these proteins contains the residues required for metal binding and substrate hydrolysis. However, the regions of these proteins that confer

specificity for individual substrates display high sequence variation.[7] Nudix enzymes play an important role in sanitization of oxidized nucleotide pools in various organisms.[4, 5] Reactive oxygen species (ROS) produced as a byproduct of cellular metabolism are capable of oxidizing free nucleotides within the cell.[8] 7,8-dihydro-8-oxo-guanine (8-oxo-G) is one of the most predominant oxidized nucleotides[9, 10] and pairs with both adenine and cytosine, resulting in transversion mutations.[11, 12] Removal of these damaged nucleotides from the nucleotide pool by Nudix proteins is essential to prevent their incorporation into DNA and RNA. This class of Nudix enzymes has been studied extensively in bacteria and humans,[7, 13-15] however little is known about the structure and function of their homologues in plants.

Nucleotide pool sanitizing enzymes play an important role in plants where even under optimal conditions metabolic processes including photosynthesis produce ROS.[16] Additionally, environmental stresses such as drought, high salinity and low temperature further increase ROS levels.[17-19] In *Arabidopsis thaliana* there are 29 proteins coding for putative Nudix hydrolases, which are located in the cytosol, mitochondria and chloroplasts.[6] Of these, only *A. thaliana* NUDT1 (AtNUDT1) has been shown to display activity against oxidized nucleotides.[20-22] AtNUDT1 hydrolyzes canonical dNTP substrates but the highest reported activity is towards 8-oxo-dGTP.[21] Expression of AtNUDT1 in an *E. coli mutT*⁻ strain devoid of its own 8-oxo-(d)GTPase activity significantly suppresses the misincorporation of 8-oxo-GTP into mRNA,[21, 22] confirming that the enzyme is a functional homologue of *E. coli* MutT. The levels of 8-oxo-guanosine in genomic DNA are also significantly increased in *A. thaliana nudt1* knockout plants when compared with the wildtype under both normal and ROS inducing conditions.[22] This supports a function of AtNUDT1 in the cellular defense against DNA and RNA damage through the sanitization of oxidized free (d)NTPs in *A. thaliana*. However, in addition to this important

role, AtNUDT1 has also been shown to have activity towards other substrates such as NADH[23] and DHNTP.[20] Recent studies have also reported that AtNUDT1 hydrolyzes non-nucleotide monoterpene substrates.[24, 25] Monoterpenes are volatiles compounds, which in plants play important roles in scent production, plant-plant interactions, communication with the surrounding environment, and in the defense against pathogens.[26, 27] The structures of AtNUDT1 in complex with the terpene substrates GPP[24] and IPP[28] were recently solved. The apo structure of AtNUDT1 was also reported alongside the IPP bound structure.[28]

Here we present the structure of AtNUDT1, in complex with the oxidized nucleotide 8-oxo-dGTP. Although AtNUDT1 demonstrates the same overall fold observed in closely related Nudix enzymes, the active site revealed previously unobserved hydrogen bonds to the 8-oxo-atom. A thorough activity screening of canonical and non-canonical nucleotide substrates demonstrated NUDT1 to have a clear preference for guanine nucleotides. Analysis of AtNUDT1 mutants indicated active site residues which influence 8-oxo-dGTP recognition. These results taken in light of recent terpene metabolism studies indicate that AtNUDT1 has evolved to have a broader function than its homologues from both humans and bacteria.

MATERIALS AND METHODS

Protein overexpression and purification of AtNUDT1. *A. thaliana nudt1* cDNA optimized for *E. coli* expression was purchased from Eurofins and subcloned into pET28a(+) (Novagen). AtNUDT1 was expressed in *E. coli* Rosetta 2 (DE3) pLysS at 17 °C for 16 hours following induction with 1 mM IPTG. Cells were harvested by centrifugation and resuspended in ice-cold lysis buffer (50 mM HEPES pH 7.5, 500 mM NaCl, 10 % (v/v) glycerol, 0.5 mM TCEP, 10 mM imidazole, 25 U/mL benzonase, 1 µl/mL Roche protease cocktail inhibitor), and then lysed via

high-pressure homogenization. The lysate was cleared using centrifugation followed by filtration through a 0.2 μm membrane filter. The sample was loaded onto a 1 mL HisTrap HP column (GE Healthcare) pre-equilibrated with running buffer (50 mM HEPES pH 7.5, 500 mM NaCl, 10 % glycerol (v/v), 0.5 mM TCEP, 10 mM imidazole). His-tagged AtNUDT1 was eluted by an increasing gradient of 0-300 mM imidazole. Fractions containing AtNUDX1 were pooled and loaded on to a Superdex 200 16/600 Size-exclusion column equilibrated with 20 mM HEPES pH 7.5, 500 mM NaCl, 0.5 mM TCEP and 5 % (v/v) glycerol. Protein purity was assessed using SDS-PAGE and mass spectrometry. Approximately 20 mg of pure AtNUDT1 was obtained per liter of culture.

Production of AtNUDT1 mutants. The mutations N76A, S89A and N76A/S89A were introduced by site-directed mutagenesis with Phusion polymerase using the method described by Li *et al.*[29] PCR was performed using the following primers: 5´-ACAAACGCGGTCTTCAAAGAAGCACCATC-3´ (AtNUDT1N76AFor), 5´-GAAGACCGCGTTTGTAACAGTCAAAAGCTT C-3´ (AtNUDT1N76ARev), 5´-TACGTCGCGGTTTCGATACGTGCGGTG-3´ (AtNUDT1S89AFor) and 5´-CGAAACCGCGACGTAGTGTGATGGCG-3´ (AtNUDT1S89ARev). Successful mutagenesis was verified by sequencing. AtNUDT1(N76A), AtNUDT1(N89A) and AtNUDT1(N76A/S89A) mutants were expressed and purified as described above for the wild type enzyme.

Crystallization and data collection. Purified AtNUDX1 (26 mg/mL) pre-incubated with 10 mM 8-oxo-dGTP and 10 mM $MgCl_2$ then crystallized via sitting drop vapor diffusion in 40 % (v/v) PEG300, 0.1 M sodium acetate/acetic acid pH 4.5 and 0.2 M NaCl. Protein crystals were flash frozen directly in liquid nitrogen without adding additional cryo-protectant solution. A native AtNUDT1 data set was collected at the European Synchrotron Radiation Facility on the

ID29 beamline ID29 equipped with a PILATUS 6M detector. A total of 200° of data was collected at 100 K at a wavelength of 1.07 Å using an oscillation angle of 0.1° and an exposure time of 0.02 s per image.

Structure determination and refinement. Data reduction and processing were carried out using XDS[30] and programs from the CCP4 suite[31]. The structure of AtNUDX1 was solved via molecular replacement with MolRep[32] using the monomer of *E. coli* MutT (PDB ID: 3A6S),[7] to which it has a sequence identity of 30 %, as the search model. This was performed assuming two monomers per asymmetric unit, in accordance with the calculated Matthews coefficient.[33] Arp/wARP[34] was used to build the initial model. After several rounds of manual model building using Coot[35] and refinement using Refmac5,[36] the electron density improved and waters, magnesium ions and finally 8-oxo-dGTP were incorporated into the structure. The final model was validated using PROCHECK,[37] with the resulting Ramachandran plot indicating that 98.5 % of the residues are in the most favored regions, with the remaining 1.5 % in additionally allowed regions. Data processing and refinement statistics are listed in Table 1. The coordinates and structure factors for the AtNUDX1 structure presented in this paper were deposited into the PDB under code 6FL4.

Substrate screen of AtNUDT1 proteins with nucleoside triphosphates. To investigate the substrate selectivity of AtNUDT1, enzyme activity was tested against a variety of canonical and oxidized adenine and guanine nucleotides (ATP, 2-OH-ATP, dATP, 2-OH-dATP, GTP, 8-oxo-GTP, dGTP, 8-oxo-dGTP). Each assay reaction consisted of reaction buffer (100 mM Tris-acetate pH 8.0, 40 mM NaCl, 10 mM Magnesium acetate, 1 mM DTT), 20 nM purified AtNUDT1 and 100 μM nucleotide substrate (listed above). An excess of *E. coli* pyrophosphatase (0.2 U/mL), produced in house,[38] was included in the assay mixture to convert formed

pyrophosphate (PP_i) into inorganic phosphate (P_i) Reaction mixtures were incubated at 25 °C for 20 minutes after which. the P_i formed was detected by the addition of malachite green reagent[39] followed by measurement of the absorption at 630 nm. To understand the function of the active site residues of Asn76 and Ser89, the mutants AtNUDT1(N76A), AtNUDT1(N89A) and AtNUDT1(N76A/S89A) were tested against the same panel of substrates using the same reaction conditions as described above.

Kinetic analysis of AtNUDT1 and AtNUDT1(N76A/S89A). To determine initial reaction rates 2 nM AtNUDT1 or AtNUDT1(N76A/S89A) was incubated in assay buffer (100 mM Tris-acetate pH 8.0, 40 mM NaCl, 10 mM Magnesium acetate, 1 mM DTT) containing either dGTP (0-300 μM) or 8-oxo-dGTP (0-60 μM) as the substrate. Reactions were carried out at 25 °C and several time points were measured over a 30 minute period. Formed pyrophosphate was detected using the PP_i Light Inorganic Phosphate Assay from Lonza according to the manufacturer's recommendations. A PP_i standard curve was included on each assay plate and used to calculate the concentration produced PP_i. Kinetic parameters were determined by fitting the Michaelis-Menten equation to initial rate data using non-linear regression and the GraphPad Prism software (GraphPad Prism, La Jolla, CA). Experiments were performed twice with data points monitored in duplicate.

Substrate screen of AtNUDT1 with nucleotide and monoterpene substrates. Hydrolysis activity of 100 nM AtNUDT1 was tested with 100 μM dGTP (Sigma-Aldrich), 8-oxo-dGTP and 8-oxo-GTP (TriLink BioTechnologies), 8-oxo-dGDP (Jena Bioscience), Geranyl-PP, Isopentenyl-PP and Farnesyl-PP (Sigma-Aldrich), Dimethylallyl-PP (Cayman Chemicals and Sigma-Aldrich) and NADH (Sigma-Aldrich). The reactions were performed at 22°C in reaction buffer consisting of 100 mM TrisAcetate pH 8.0, 40 mM NaCl and 10 mM MgAcetate. Samples

with dGTP, 8-oxo-dGTP and 8-oxo-GTP contained an excess of *E. coli* PPase (0.2 U/mL) to convert the reaction product PPi into Pi. After 30 minutes formed Pi was detected by addition of malachite green reagent followed by incubation with shaking for 15 minutes after which absorbance was read at 630 nm. Absorbance was converted to concentration formed Pi by using a Pi standard curve.

Table 1. Data collection and refinement statistics

PDB code	6FL4
Data collection	
Space group	*I*222
Cell dimensions:	
a, b, c (Å)	64.9, 77.4, 122.4
α, β, γ (°)	90, 90, 90
No. of observations	300101 (13865)
No. of unique reflections	41032 (1950)
Resolution (Å)	38.7-1.6 (1.69-1.60)
R_{sym} or R_{merge}	0.12 (0.68)
CC(1/2) (%)	99.7 (83.4)
$I / \sigma I$	9.0 (1.9)
Completeness (%)	99.5 (98.4)
Redundancy	5.7 (5.6)
Refinement	
Resolution (Å)	38.7-1.6
No. of reflections	41078
R_{work} / R_{free}	17.9/21.4

No. of atoms:	
Protein	2231
Ligand/ion	68
Water	251
ADPs (Å^2):	
Protein	17.4
Ligand/ion	28.4
Water	27.6
R.m.s. deviations:	
Bond lengths (Å)	0.011
Bond angles (°)	1.69

Values in parenthesis are for the highest resolution shell.

RESULTS

Overall structure of AtNUDT1. The structure of AtNUDT1 in complex with 8-oxo-dGTP was solved to 1.60 Å resolution. A structural similarity search was performed using the DALI web server,[40] which verified that AtNUDT1 is most structurally similar to other enzymes of the Nudix superfamily. The enzyme displayed high Z-scores with human MTH1 and the *E. coli* homologue MutT, which was the first of these enzymes to be structurally and kinetically characterized and found to catalyze the hydrolysis of 8-oxodGTP.[7] The tertiary structure of AtNUDT1 is a homodimer (Figure 1). This dimeric tertiary structure is consistent with biochemical studies of AtNUDT1, which have verified the protein to be dimeric in solution.[23] This observation contrasts with human MTH1 and MutT, which are both monomeric in solution.[7, 13] Analysis of the AtNUDT1 dimer interface with PISA (Protein interfaces, surfaces and assemblies) of the EBI webserver[41] demonstrates a solvation-free energy gain of 18.5 kcal

mol^{-1} and a *P* value upon dimer formation of 0.015, with an interface area of 921.8 Å^2. There are 24 residues from each monomer, which contribute to the dimer interface of AtNUDT1.

The AtNUDT1 monomer is composed of two α-helices (α1 and α2) and six β-strands (β1 to β7) and has an α/β/α sandwich structure conserved amongst members of the Nudix family (Figure 1A).[7, 13] The individual monomers of AtNUDT1 are very similar to one another with a low rmsd value of 0.31 Å for the corresponding Cα-atoms. The highly conserved Nudix motif ($GX_5EX_7REUXEEXGU$) is located on α-helix 1 and β-strand 4 and contains the residues required for metal binding and substrate hydrolysis. There is one 8-oxo-dGTP ligand and two magnesium ions per substrate binding site, the latter of which exhibits octahedral coordination to the ligand, several water molecules, and the Nudix motif (Figure 1B). The structure of apo AtNUDT1 (PDB ID: 6DBY) was recently reported.[28] Comparison of this structure with the 8-oxo-dGTP bound enzyme indicates that there are no major conformational changes induced upon ligand binding, nor are there significant changes in the active site binding pocket (Supplementary Figure 1).

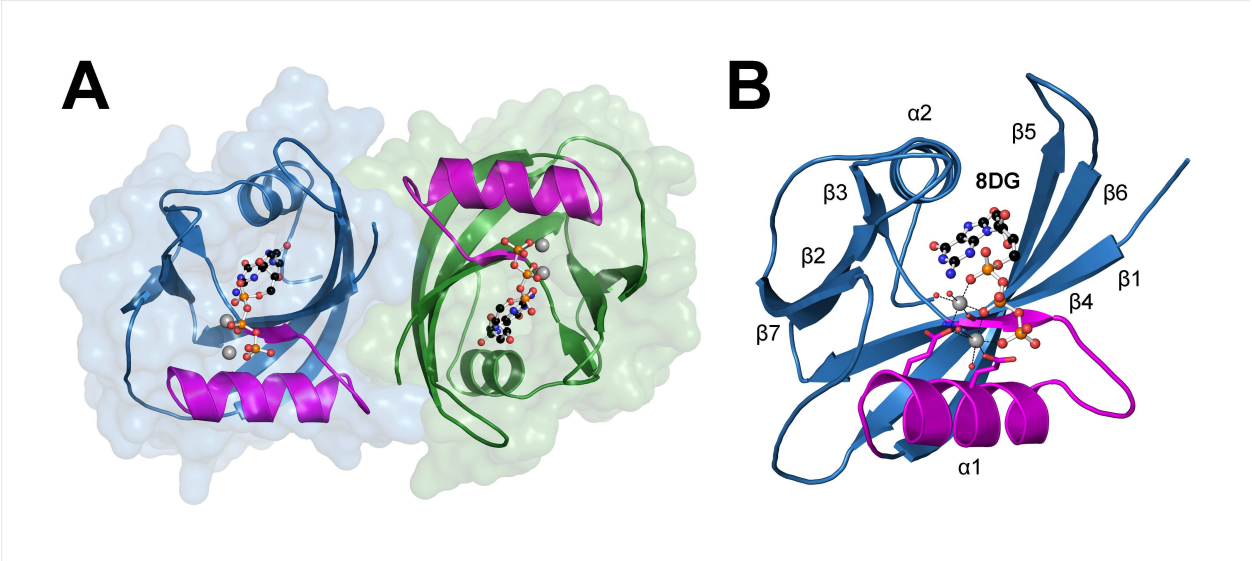

Figure 1. Crystal structure of the AtNUDT1 8-oxo-dGTP complex. (A) Crystallographic structure of dimeric AtNUDT1. Individual monomers are shown as ribbon representations, colored blue and green. The Nudix motif of each monomer is colored magenta. The 8-oxo-dGTP (8DG) ligands are depicted as ball-and-stick models; C atoms are colored black, O atoms red, N atoms blue and P atoms orange. Magnesium ions involved in ligand coordination are shown as gray spheres. The surface representations for individual monomers are shown in blue and green. (B) Ribbon representation of the AtNUDT1 monomer. The color-scheme and depictions of the Nudix motif, 8DG and magnesium ions are the same as those used in Figure 1A. The secondary structure elements, α-helices (1-2) and β-strands (1-7) are labeled. The main-chain atoms of Gly40 and side-chains atoms of Glu56 and Glu60 involved in magnesium ion co-ordination are shown as sticks, with O and N atoms colored red and blue, respectively.

8-oxo-dGTP recognition by AtNUDT1. The AtNUDT1 structure shows clear density for 8-oxo-dGTP, which binds the enzyme in the *syn* glycosidic conformation (Figure 2). During refinement there was clear electron density for the α-phosphate of dGTP, however the β-phosphate and γ-phosphate of the ligand were placed at partial occupancy (90 and 75 %, respectively). This was achieved by refinement of the atoms at different occupancies followed by visual inspection of the resulting electron density maps. The ADP values for the α- β- and γ-phosphates were 23.0, 25.5 and 39.7 $Å^2$, respectively. These values are higher than the average ADP value of 15.4 $Å^2$ observed for the surrounding protein side chains (Figure 2). The values for the α- and β-phosphate were comparable to the base (20.2 $Å^2$) and deoxyribose moieties (23.4 A^2) of 8-oxo-dGTP, whereas the ADP value observed for the γ-phosphate was significantly higher. This observation could be due to partial hydrolysis of the substrate and/or radiation damage. The β- and γ-phosphates of the nucleotide are not always completely cleaved in the

crystal structures of these enzymes, as there are structures of human MTH1 in the protein databank in complex with 8-oxo-dGTP.[42, 43] Both magnesium ions in the AtNUDT1 structure exhibit ideal octahedral coordination to several water molecules, 8-oxo-dGTP and residues of the Nudix motif. Specifically, Mg1 hydrogen bonds the side chain of Glu56 and Glu60, two water molecules and an oxygen atom from both the β- and γ-phosphate of 8-oxo-dGTP. Mg2 is coordinated with the side chain of Glu60, the main chain oxygen of Gly40, two water molecules and an oxygen atom from both the α- and β-phosphate of the ligand (Figure 2). In addition to magnesium ion coordination, the α-phosphate is within bonding distance (closer than 3.1 Å) to the side chain of Arg27, two water molecules and to the N3 atom of the 8-oxo-guanine base. The β-phosphate is within range of the side chains of Lys110 and His42, a water molecule, and the main chain oxygen of Gly40. The γ-phosphate also hydrogen bonds to the side chain of Glu56, the main chain nitrogen atom of His42, and three water molecules. The deoxyribose moiety of 8-oxo-dGTP is positioned by a C-H···π interaction with Tyr87 and the O3' atom is also within bonding distance of a water molecule and the side chain of Arg27. The 8-oxo-guanine base of the ligand makes several hydrogen bond interactions with three water molecules, the main chain nitrogen and oxygen atoms of Leu38, and the side chains of Asn76, Ser89 and Arg27 (Figure 2). The hydrogen bonding between Ser89 and Asn76 with the O8 atom of 8-oxo-dGTP is a particularly interesting feature. The structures available for related enzymes such as *E. coli* MutT and human MTH1 in complex with the ligand show no such interactions at this position.[7, 13, 42, 43] Based on this observation we made single and double mutants at these positions to assess the role Asn76 and Ser89 play in the recognition of oxidized and non-oxidized nucleotides by AtNUDT1. Structures of human, mouse, dog and zebrafish MTH1 (NUDT1) have been determined, they all

display highly similar substrate binding pockets, clearly distinct from the AtNUDT1 complex presented here.[13, 14, 44, 45]

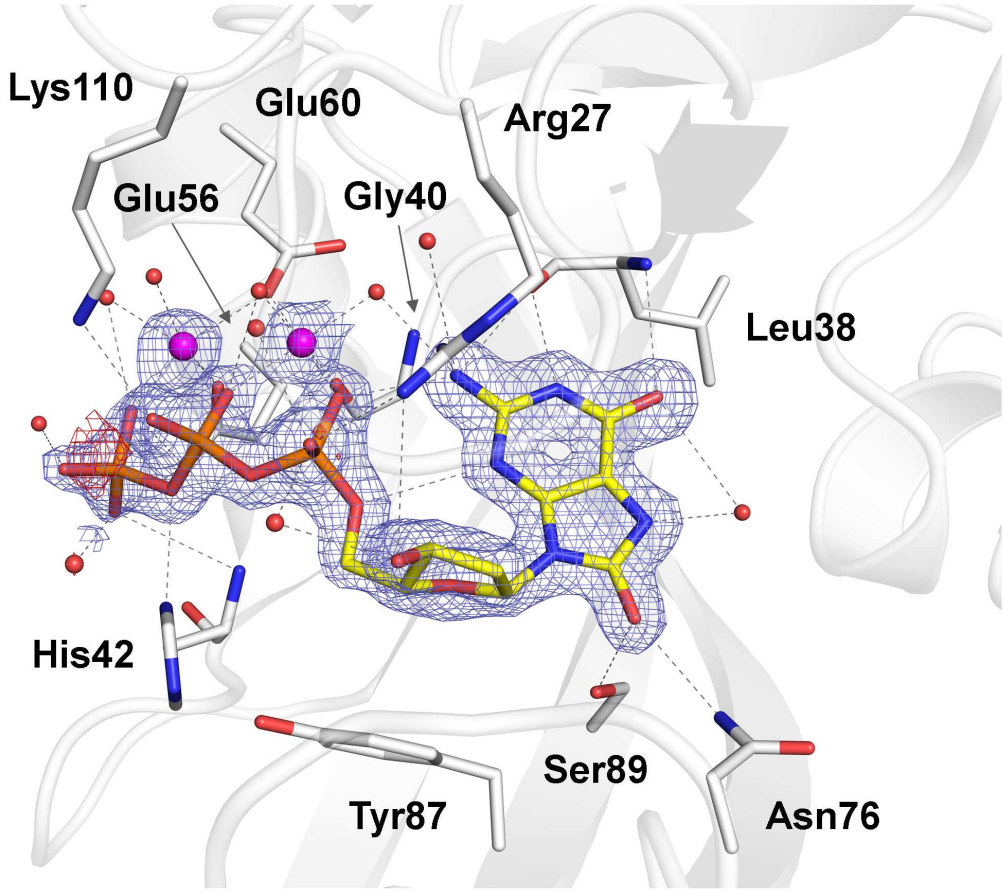

Figure 2. The recognition of 8-oxo-dGTP by AtNUDT1. The active site hydrogen bond network of AtNUDT1 with 8-oxo-dGTP bound in the *syn* glycosidic conformation. Amino acids contributing to ligand binding are depicted as sticks; C atoms are colored white, O atoms red and N atoms blue. 8-oxo-dGTP is presented as a stick model; C atoms are colored yellow, O atoms red and N atoms blue, P atoms orange. Magnesium ions involved in ligand coordination are shown as magenta spheres. Important water molecules that are alluded to in the text are shown as red spheres. Hydrogen bond interactions are shown as dashed lines. The $2F_o$- F_c electron density

map around 8-oxo-dGTP contoured at 1.5 σ and the F_o - F_c electron density map is contoured at 3.0 σ.

Nucleotide substrate preferences of wild-type and mutant AtNUDT1. To investigate the substrate selectivity of AtNUDT1, enzyme activity was tested against a variety of canonical and oxidized adenine and guanine nucleotides (ATP, 2-OH-ATP, dATP, 2-OH-dATP, GTP, 8-oxo-GTP, dGTP, 8-oxo-dGTP). AtNUDT1 demonstrated a clear preference for guanine nucleotides, having similar activities for 8-oxo-GTP, dGTP and 8-oxo-dGTP, but less activity towards GTP (Figure 3A). AtNUDT1 also displayed significant activity towards dATP as has been observed previously[21] but did not hydrolyze any of the other adenosine nucleotide substrates tested. In contrast to its *E. coli* homologue MutT,[12] AtNUDT1 did not show a strong preference for 8-oxo-dGTP over the non-oxidized form. When compared to the human homologue MTH1, the activity of AtNUDT1 for the substrates tested was shown to be significantly lower, and was much less specific for oxidized nucleotides (Supplementary Figure 2). As detailed above, in our AtNUDT1 structure we noted hydrogen bond interactions between Ser89 and Asn76 with the O8 of 8-oxo-dGTP, a feature not observed in other MutT homolog structures solved to date.[7, 13, 42, 43] Single and double mutants of these residues were produced and tested against the same panel of nucleotides as performed for wild-type AtNUDT1 (Figure 3B). When examining the hydrolysis of guanine nucleotides by the single mutants, the S89A mutant had slightly more of an effect on catalysis than N76A, which generally retained activity almost identical to wild-type AtNUDT1. The double mutant showed a minor decrease in activity compared to the wild-type and N76A single mutant. Although, the slight drop in activity observed for the double mutant was often comparable to the S89A single mutant alone (Figure 3B). Interestingly, when examining the hydrolysis of canonical and oxidized adenosine nucleotides, the S89A mutant showed a slight

increase in activity compared to the wild-type enzyme for ATP, dATP and 2-OH-dATP. However, the single N76A and the double AtNUDT1 mutant generally retained activity similar to the wild-type protein (Figure 3B).

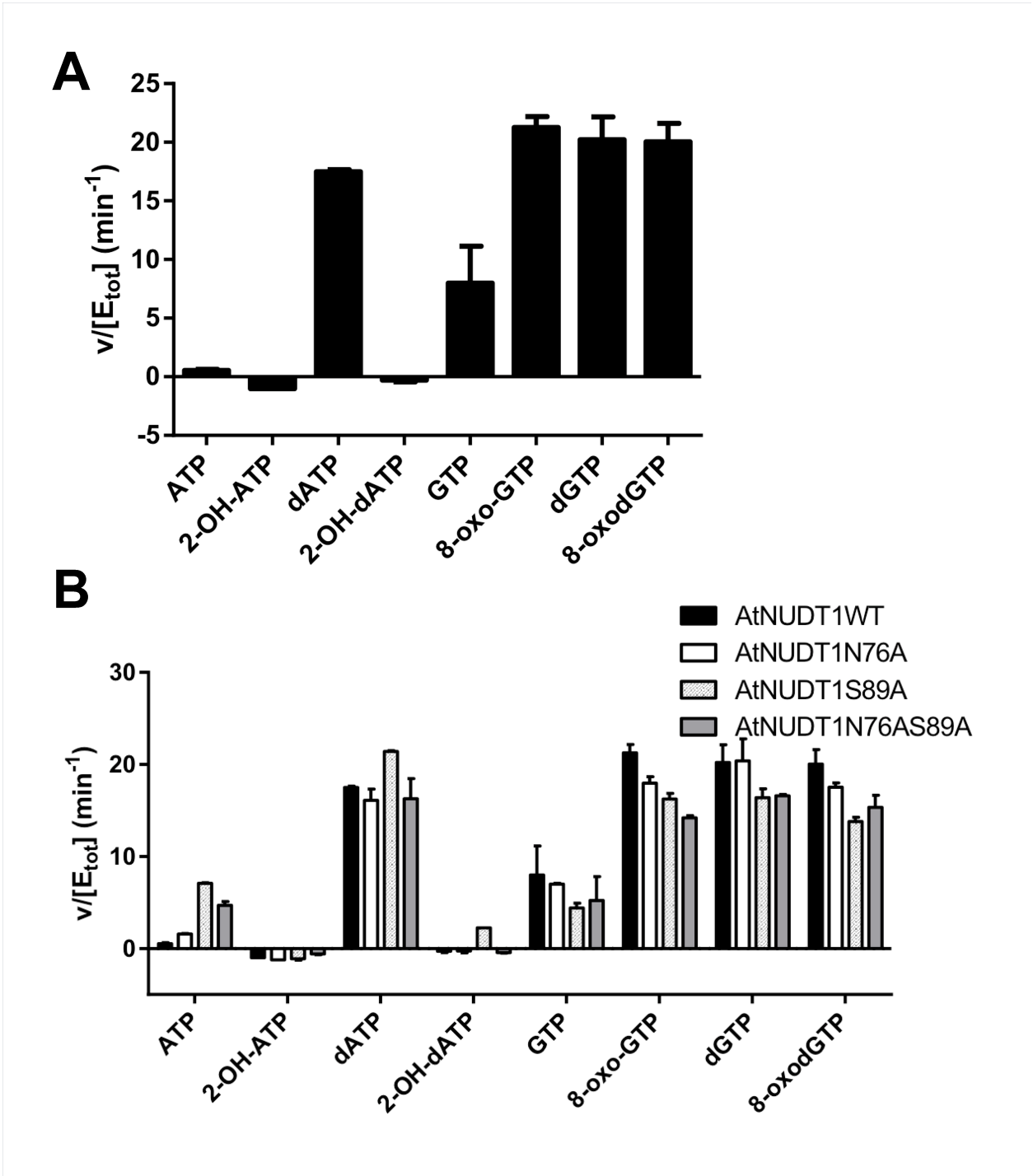

Figure 3. Substrate screen of AtNUDT1 and AtNUDT1 mutants. (A) The activity of wild-type AtNUDT1 tested against a panel of canonical and oxidized adenine and guanine nucleotides. (B) Comparison of activities between wild-type AtNUDT1 and AtNUDT1 active site mutants, with the same panel of substrates shown in A. Assays were performed in duplicate at 25 °C. Formed P_i was detected using Malachite green reagent and absorbance values were measured at 630 nm. Data are presented as *v* (hydrolyzed substrate (μM) per minute) per [enzyme] (μM).

Kinetics of wild-type and mutant AtNUDT1 with 8-oxo-dGTP and dGTP. Overall, the single and double mutants did not cause a dramatic decrease in activity for any of the nucleotides tested, likely due to the substrate saturating conditions used in these assays (Figure 3). In order to properly understand the role of the N76A and S89A active site mutants in the specificity of AtNUDT1 for oxidized guanine nucleotides, a more careful kinetic analysis was performed. AtNUDT1 wild-type and the N76A and S89A double mutant were assayed against various concentrations of dGTP and 8-oxo-dGTP, and kinetic constants were determined (Figure 4A). The K_m values of wild-type AtNUDT1 for 8-oxo-dGTP and dGTP were analogous, indicating no difference in affinity for the two substrates. The values for k_{cat}/K_m however, which represents the catalytic efficiency of a reaction, indicated a 1.5 fold higher catalytic efficiency with 8-oxo-dGTP compared to dGTP (Figure 4B). A previously published study showed AtNUDT1 to have a roughly 8-fold lower K_m value for 8-oxo-dGTP compared to dGTP, something that was not observed in this analysis. The catalytic efficiency of AtNUDT1 calculated in that study was roughly 2.5-fold higher for the oxidized nucleotide, a value slightly higher than what is reported here.[21] The K_m values for the AtNUDT1 double mutant showed a 2.6 and 2.3-fold increase compared to the wild-type protein for 8-oxo-dGTP and dGTP, respectively (Figure 4A)

indicating that removal of the hydrogen bond donors as in the double mutant does not have a major impact on binding of the 8-oxo-dGTP substrate specifically. However, the relative catalytic efficiency of the double mutant for 8-oxo-dGTP was 3-fold lower than for the wild-type enzyme, whereas being only 1.3-fold lower for dGTP (Figure 4B) implying that these mutations do have an effect on the relative catalytic efficiencies of these substrates.

A

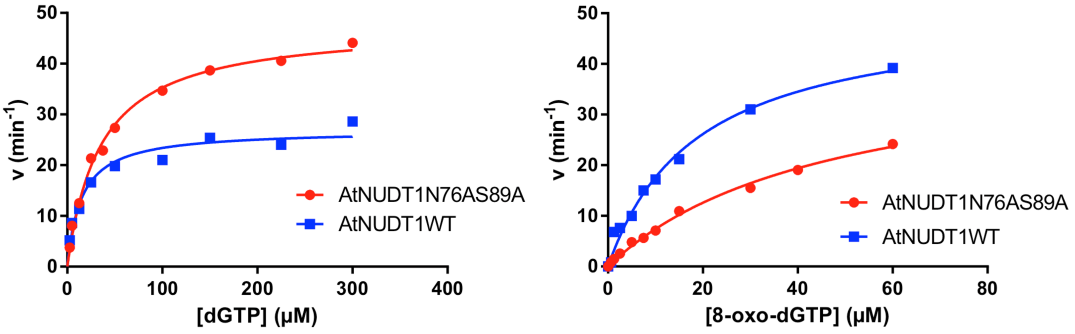

B

Protein	K_m (μM)	k_{cat} (s^{-1})	k_{cat}/K_m ($M^{-1}s^{-1}$)
AtNUDT1(WT)			
8-oxo-dGTP	18.8 ± 2.7	0.85 ± 0.05	$4.50 \cdot 10^4$
dGTP	15.0 ± 3.1	0.45 ± 0.02	$2.99 \cdot 10^4$
AtNUDT1(N76A/S87A)			
8-oxo-dGTP	47.1 ± 5.6	0.70 ± 0.05	$1.49 \cdot 10^4$
dGTP	35.0 ± 3.1	0.79 ± 0.02	$2.27 \cdot 10^4$

Figure 4. Enzyme kinetics of wild-type and mutant AtNUDT1 with dGTP and 8-oxo-dGTP. (A) Saturation curves of wild-type AtNUDT1 (AtNUDT1WT) and AtNUDT1 mutant (N76A/S89A) mediated hydrolysis of dGTP (left) and 8-oxo-dGTP (right). Each enzyme (2 nM) was incubated with concentrations of dGTP and 8-oxo-dGTP ranging from 0-300 μM and 0-60 μM, respectively. Substrate hydrolysis was determined by measuring PP_i formation, which was detected using the PPiLight Inorganic Pyrophosphate Assay (Lonza). Data are presented as v (hydrolyzed substrate (μM) per minute) per [enzyme] (μM). Initial reaction rates were

determined in duplicate. (B) Kinetic parameters of AtNUDT1WT and the AtNUDT1(N76A/S89A) mutant for dGTP and 8-oxo-dGTP hydrolysis. Kinetic values were determined by fitting the Michaelis-Menten equation to the initial reaction rates using GraphPad Prism. Data presented are the average ± s.d. from two independent experiments.

Structural comparison of AtNUDT1 with related Nudix enzymes. Comparison of the AtNUDT1 monomer with homologues from humans and bacteria indicates that these enzymes share the same overall structure (Figure 5A). Following Cα atom superposition, AtNUDT1 displays similar r.m.s.d values when compared to *E. coli* MutT (1.74 Å) and human MTH1 (1.81 Å) with which it shares a similar level of sequence identity (30 % and 26 %, respectively). The Nudix motifs, containing residues critical for metal binding and substrate hydrolysis, located on α-1, β-4 and the connecting loop region, superimpose well (Figure 1, Figure 5A). In general, the core secondary structure elements of the enzymes overlay nicely. The exceptions are a few loop regions distant to the active site, but more importantly, the position of α-helix 2 (Figure 5A). The positioning of this α-helix in AtNUDT1 differs most with human MTH1 reflecting the differences in nucleotide binding within the active sites. As noted in the previous section, AtNUDT1 has much lower activity compared to both *E. coli* MutT and human MTH1, and is much less specific towards oxidized nucleotides. A major difference between these proteins is their tertiary structure, human MTH1 and *E. coli* MutT both being monomeric in solution[7, 13] whereas AtNUDT1 forms a homodimer in solution.[23] However, this difference is unlikely to be responsible for the kinetic differences, as mutational studies of the AtNUDT1 dimer interface have indicated that its disruption does not affect catalysis.[24] Additionally, it is evident from the AtNUDT1 structure, that the location of the dimer interface is distant to the substrate-binding site (Figure 1A). When comparing the active site of AtNUDT1 to *E. coli* MutT and human

MTH1 following Cα atom superposition, the plant enzyme was shown to be much more similar to the bacterial enzyme (Figure 5B,C). In the AtNUDT1 structure the 8-oxo-dGTP ligand binds in the *syn* glycosidic conformation. This is the same conformation as observed for 8-oxo-dGTP bound *E. coli* MutT (Figure 5B) and contrasts to human MTH1 where the ligand binds the protein in the *anti* glycosidic conformation (Figure 5C). As noted previously, a key difference between AtNUDT1 and these structures is the hydrogen bond interactions between Asn76 and Ser89 with the O8 position of 8-oxo-dGTP (Figure 2). Such a direct interaction with the oxidized component of the ligand is not observed in the bacterial and human homologues.[7, 13] In *E. coli* MutT the residues equivalent to Asn76 and Ser89 of AtNUDT1 are Tyr73 and Leu82, neither of which are within hydrogen bonding distance to O8. The hydroxyl group of the tyrosine points in the opposite direction of 8-oxo-dGTP, and no atoms from the main chain of either amino acid are within binding range to the ligand (Figure 5B). This is a similar observation to the human MTH1 structure where the equivalent positions are occupied by two hydrophobic residues (Phe73 and Val83), which form part of a hydrophobic pocket (Figure 5C).

Comparison of the AtNUDT1 and *E. coli* MutT active sites indicates that the base and deoxyribose moieties of the 8-oxo-dGTP ligand superimpose well. The amino acids involved in substrate recognition also adopt similar overall positions, however their chemical properties differ significantly (Figure 5B). For example, there are several hydrophobic residues in AtNUDT1, namely Ile31, Ala37 and Leu130, which are hydrophilic residues in *E. coli* MutT (His28, Glu34 and Asn119, respectively). There is also a C-H···π interaction between Tyr87 in AtNUDT1 and the deoxyribose moiety of 8-oxo-dGTP, which is absent in MutT where there is a hydrophobic residue (Ile80) located at the equivalent position (Figure 5B).

However a pi-stacking interaction is observed in the human MTH1 structure between Phe72 and the base of the nucleotide (Figure 5C). When analyzing the superposition of AtNUDT1 with human MTH1 it is evident that in spite of their similar overall structures, their active site hydrogen bond networks differ significantly (Figure 5C). An important difference is the movement of α-helix 2 in human MTH1, which positions two aspartate residues (Asp119 and Asp120) for nucleotide binding. These amino acids play important roles in human MTH1 substrate specificity.[43, 46] The human MTH1 enzyme has a broader substrate selectivity for oxidized nucleotides and can in contrast to AtNUDT1 also effectively hydrolyze oxidized adenosine nucleotides such as 2-OH-dATP in addition to its 8-oxo-dGTP activity (Supplementary Figure 2). Previous mutational and crystallographic studies have proposed that human MTH1 recognizes 8-oxo-dGTP *via* protonated Asp119 and deprotonated Asp120, which switches in order to enable the recognition of 2-OH-dATP.[43, 46] There are no equivalent residues at these positions in AtNUDT1. However, despite differences in binding of the base and deoxyribose moieties of 8-oxo-dGTP, the positions of the phosphates and metal ions in these structures are comparable (Figure 5B,C). Therefore, the site of hydrolysis is conserved between these enzymes even if the regions determining substrate specificity are not. The residues Gly40, Glu56 and Glu60, involved in metal ion coordination (Figure 2), superimpose particularly well between the structures. These amino acids are part of the highly conserved Nudix motif characteristic of this family of enzymes.

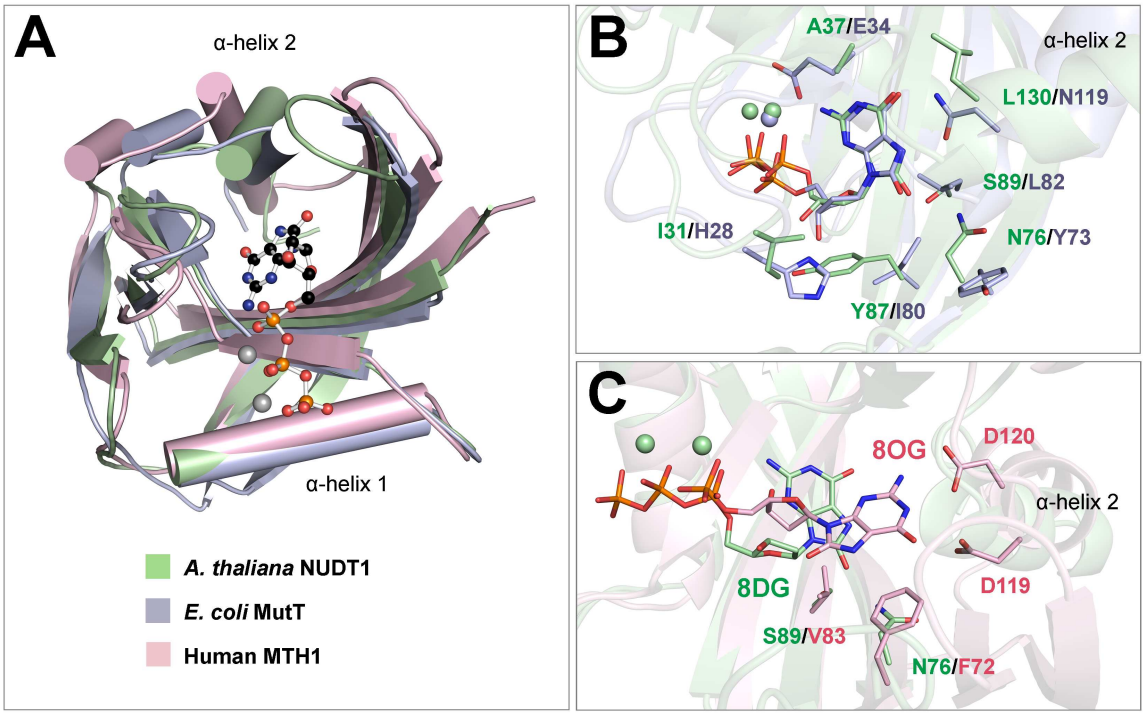

Figure 5. Comparison of AtNUDT1 with closely related Nudix enzymes. (A) Cα-atom superposition of whole monomers visualized as ribbon representations. AtNUDT1 (green), *E. coli* MutT (purple) and human MTH1 (pink). The 8-oxo-dGTP ligand of AtNUDT1 is depicted as a ball and stick model; C atoms colored black, O atoms red, N atoms blue and P atoms orange. The magnesium ions of AtNUDT1 are shown as gray spheres. (B) Comparison of the AtNUDT1 active site (green) with *E. coli* MutT (purple). The 8-oxo-dGTP of AtNUDT1 and 8-oxo-dGMP of MutT are shown in the *syn* glycosidic conformation. (C) Overlay of the AtNUDT1 active site (green) with 8-oxo-dGTP in the *syn* conformation and hMTH1 (pink) with 8-oxo-dGMP in the *anti* conformation. In panels B-C, the metal ions of AtNUDT1 and MutT are depicted as spheres. Amino acids are depicted as sticks; O atoms red, N atoms blue and the carbon atoms of AtNUDT1, MutT and hMTH1 shown in green, purple and pink, respectively.

Comparison of AtNUDT1 activities and structures involving terpenes. We tested the activities of AtNUDT1 with previously described substrates of AtNUDT1 under the same assay conditions (Figure 6A). Based on published Km values[21, 25] the used substrate concentration of 100 μM is well above the Km values resulting in the enzyme being saturated with substrate. Under these conditions 8-oxodGTP, dGTP as well as 8-oxoGTP, are hydrolyzed to approximately the same extent and are clearly turned over faster than the monoterpene substrates and NADH. However, since the monoterpene substrates display lower Km values compared to 8-oxo-dGTP[25] the catalytic efficiency for 8-oxo-dGTP is approximately the same as for the monoterpene substrates. Aiming to explain the difference in binding affinity between 8-oxo-dGTP and the monoterpene substrates to AtNUDT1 reflected in the lower Km values for the monoterpene substrates, we compared our structure with AtNUDT1 in complex with 8-oxo-dGTP with the published structures of AtNUDT1 in complex with GPP[24] and IPP.[28] GPP belongs to the monoterpene family of volatiles, which play important roles in the defense against pathogens, pollinator attraction, plant-plant interactions and communication with the surrounding environment in plants.[26, 27] In addition to their roles in plants, derivatives of monoterpenes have widespread use in fragrances, flavors and in the pharmaceutical industry.[47]

Superposition of the individual AtNUDT1 monomers bound with 8-oxo-dGTP, GPP and IPP indicates that there are no major conformational differences between these structures (Figure 6B). Comparison of our AtNUDT1 8-oxo-dGTP complex with the AtNUDT1 GPP (PDB ID: 5GP0) bound structure shows the two substrates utilize the same binding site (Figure 6C). These structures are highly similar as indicated by the low r.m.s. differences of 0.578 Å for their individual monomers. The GPP bound structure contains the mutation Glu56A which renders the enzyme completely catalytically inactive.[24] Interestingly, GPP adopts two alternate

conformations in the active site. In the first orientation, the geranyl component of GPP occupies a similar position to the base and deoxyribose moiety of 8-oxo-dGTP. In the second conformation the geranyl part of the ligand is directed towards a hydrophobic cavity consisting of residues Leu38, Phe78, Pro129 and Phe127. Overall the residues of the AtNUDT1 GPP active site superimpose very well with those of the 8-oxo-dGTP structure (Figure 6C). In contrast to the extensive hydrogen bond network shown in the 8-oxo-dGTP complex (Figure 2), only three amino acids (Arg27, His42 and Tyr87) form hydrogen bond interactions with GPP. Mutations to any of these three residues largely abolished GPP activity.[24] In addition, the pyrophosphate component of GPP is significantly shifted when compared to the positioning of the 8-oxo-dGTP phosphates. This is accompanied by the slight movement of Tyr87 and the flipping of His42 which allows for hydrogen bonding to the terminal phosphate of GPP (Figure 6C). There are no metal ions bound in AtNUDT1 GPP active site.

Superposition of the AtNUDT1 8-oxo-dGTP structure with IPP bound AtNUDT1 (PDB ID: 6DBZ) shows the structures are highly similar, as indicated by the low r.m.s. difference of 0.340 Å for their individual monomers. In contrast to what was observed for GPP, IPP adopts a single conformation in the active site. The terpene substrate superimposes perfectly with the α- and β-phosphates and deoxyribose moiety of 8-oxo-dGTP (Figure 6D). There are 3 magnesium ions in the active site of the IPP complex, one more than was observed for the 8-oxo-dGTP bound structure. The additional magnesium ion occupies the same position as the γ-phosphate in the AtNUDT1 8-oxo-dGTP structure. The three magnesium ions all exhibit ideal octahedral coordination (Figure 6D). The residues involved in metal ion coordination superimpose very well with the exception of Lys110 which in the 8-oxo-dGTP bound structure directly interacts

with a magnesium ion. In the AtNUDT1 IPP structure Lys110 hydrogen bonds to a water molecule, which in turn interacts with the equivalent magnesium ion (Figure 6D).

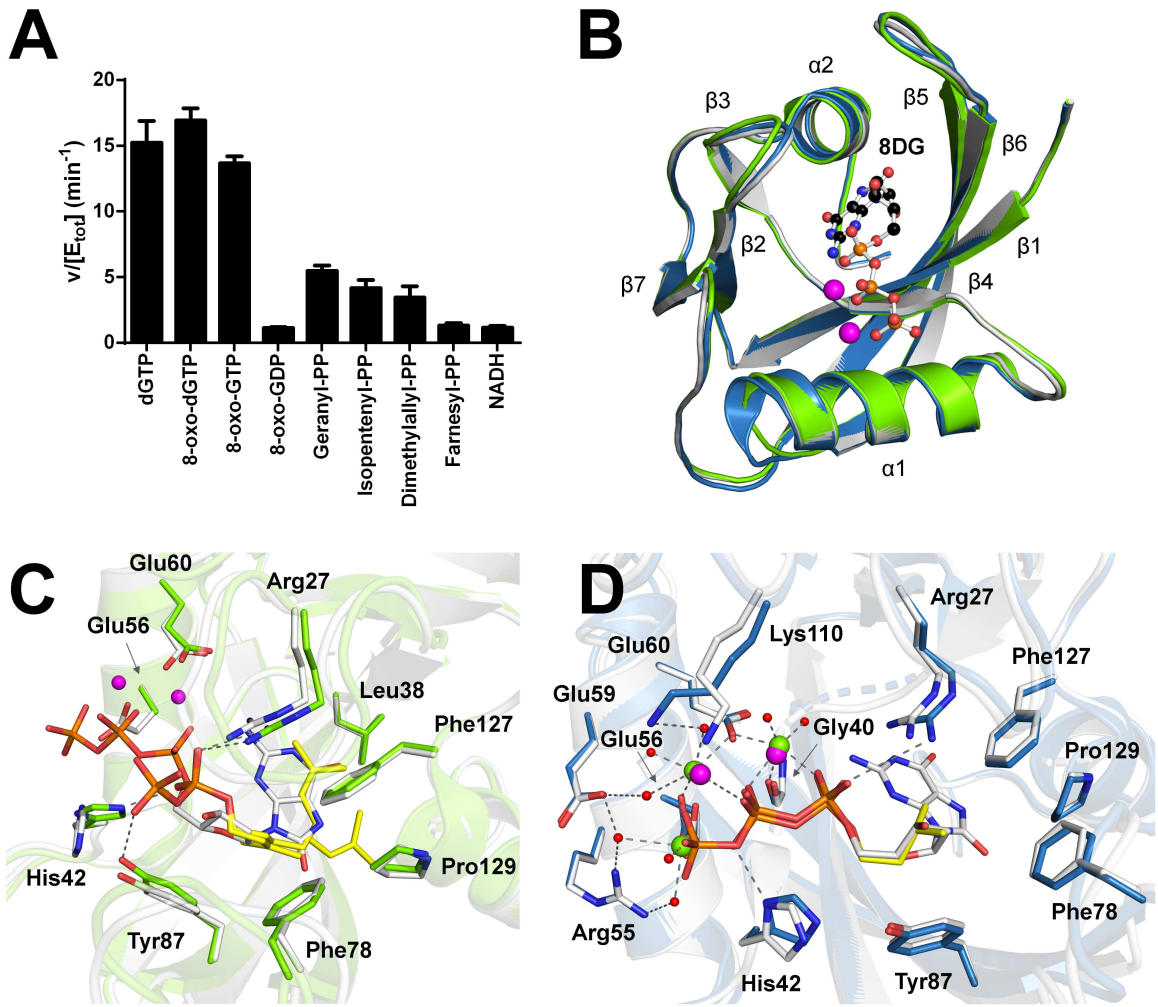

Figure 6. Comparison of AtNUDT1 activities and structures involving terpenes. (A) Substrate screen of AtNUDT1 at 100 μM substrate performed at 25°C and pH 8.0. Data are presented as v [hydrolysed substrate] (μM) per [E_{tot}] (μM) per minute. (B) Cα-atom superposition of whole monomers visualized as ribbon representations. AtNUDT1 8-oxo-dGTP (white), AtNUDT1 GPP (green) (PDB ID:5GP0) and AtNUDT1 IPP (blue) (PDB ID:6DBZ). The 8-oxo-dGTP ligand is depicted as a ball and stick model; C atoms colored black, O atoms red, N atoms

blue and P atoms orange. The magnesium ions which coordinate 8-oxo-dGTP are shown as magenta spheres. The secondary structure elements, α-helices (1-2) and β-strands (1-7) are labelled. (C) Cα-atom superposition of AtNUDT1 8-oxo-dGTP (white) with AtNUDT1 GPP (green). GPP is shown as a stick model; C atoms are colored yellow, O atoms red, P atoms orange. Hydrogen bond interactions involved in GPP binding are shown as dashed lines. The magnesium ions of the AtNUDT1 8-oxo-dGTP structure are shown as magenta spheres. (D) Cα-atom superposition of AtNUDT1 8-oxo-dGTP (white) with AtNUDT1 IPP (blue). IPP is shown as a stick model; C atoms are colored yellow, O atoms red, P atoms orange. Hydrogen bond interactions involved in IPP binding are shown as dashed lines. The magnesium ions of AtNUDT1 8-oxo-dGTP (magenta) and AtNUDT1 IPP (green) are depicted as spheres. In panels C-D amino acids are shown as sticks; O atoms red, N atoms blue, P atoms orange and the carbon atoms of AtNUDT1 8-oxo-dGTP, AtNUDT1 GPP and AtNUDT1 IPP are shown in white, green and blue, respectively.

DISCUSSION

Nudix enzymes play an important role in the removal of mutagenic dNTPs such as 8-oxo-dGTP, which prevents their incorporation into DNA. These enzymes generally prefer oxidized nucleotides but can also hydrolyze normal dNTPs, which are far more abundant *in vivo*. We have determined the structure of AtNUDT1 in complex with 8-oxo-dGTP and carried out substrate screening and characterization with various nucleotides. To date, AtNUDT1 is the only Nudix enzyme from *A. thaliana* reported to have activity against oxidized guanosine nucleotides. Analysis of the AtNUDT1 active site revealed a previously unobserved feature, hydrogen bonding between Asn76 and Ser89 to the O8 atom of 8-oxo-dGTP. Such a direct interaction has not been observed in the structures of the homologues human MTH1 and *E. coli* MutT, both of

which display high specificity towards oxidized nucleotides. Interestingly, the kinetic analysis of wild-type AtNUDT1 presented here showed only a 1.5-fold higher catalytic efficiency for 8-oxo-dGTP compared to the non-oxidized form. This does not indicate a strong preference for 8-oxo-dGTP to be compared with the preference for 8-oxo-dGTP over dGTP for the *E. coli* MutT protein that was reported to be roughly 34,000-fold.[48, 49] Neither did we observe the 8-fold lower *K*m for the oxidized nucleotide that has been described previously[21]. This suggests that AtNUDT1 is likely to have evolved to fulfill other roles in the plant cell apart from sanitizing the cell from 8-oxo-dGTP. We produced AtNUDT1 single and double mutants of Asn76 and Ser89 to further probe their role in substrate specificity. The Km value of the AtNUDT1 double mutant for 8-oxo-dGTP and dGTP was decreased by roughly 2.5 fold in both cases, which indicates that these residues do not dramatically affect substrate binding. The relative efficiency of reaction however, was decreased more for 8-oxo-dGTP than for dGTP, indicating that Asn76 and Ser89 do play a role in the catalysis of 8-oxodGTP hydrolysis in *A. thaliana*. The lack of amino acid residues able to form hydrogen bonds to O8 in in the corresponding positions in MutT and human MTH1 suggest that these residues are of minor importance for efficient catalysis of 8-oxo-dGTP.

Comparisons of AtNUDT1 with the structures of closely related *E. coli* MutT and human MTH1 demonstrated a shared overall fold. The active site residues from the characteristic Nudix motif, responsible for metal ion coordination and substrate hydrolysis, displayed strong conservation. Overall, the active site of AtNUDT1 showed more structural similarity to *E. coli* MutT with 8-oxo-dGTP binding in the *syn* conformation rather than the *anti* conformation observed for human MTH1. The 8-oxo-dGTP ligands superimposed particularly well between AtNUDT1 and MutT. However, while the overall positions of amino acids involved in substrate

recognition were similar, their chemical properties differed considerably. In particular, there were several hydrophobic residues in AtNUDT1 which were replaced by hydrophilic residues in the *E. coli* enzyme. This feature was more marked in comparisons with human MTH1, where the hydrogen bond network for 8-oxo-dGTP was drastically different to AtNUDT1. It is interesting that *E. coli* MutT and human MTH1 display a much stronger preference for 8-oxo-dGTP than AtNUDT1, in spite of their lack of direct interactions with the oxidized O8 atom of the nucleotide.

Crystal structures of *E. coli* MutT determined in the presence and absence of 8-oxo-dGMP show significant ordering of flexible loop regions surrounding the ligand.[7] The *syn* glycosidic conformation is thought to be preferred by oxidized nucleotides.[7] There are no major structural changes that occur upon 8-oxo-dGTP binding in the human MTH1 structure.[13] The specificity of human MTH1 for 8-oxo-dGTP is thought to be influenced by the stabilization of the 6-enol-8-keto tautomer of the nucleotide.[50] However, these factors do not fully explain the selectivity MutT and human MTH1 display for 8-oxo-dGTP over dGTP.

In the current study AtNUDT1 showed a clear preference for guanine nucleotides and in contrast to human MTH1, was not active against oxidized adenine species such as 2-OH-dATP.[51, 52] Mutational and crystallographic studies have proposed that human MTH1 recognizes 8-oxo-dGTP and 2-OH-dATP by the exchange of protonation states between Asp119 and Asp120.[43, 46] AtNUDT1 lacks these residues, which in human MTH1 are located on an α-helix, the position of which is significantly shifted compared to the plant enzyme. These factors could contribute to the inability of AtNUDT1 to hydrolyze oxidized adenine nucleotides. AtNUDT1 was also significantly less active than human MTH1 against several oxidized nucleotides (Supplementary Figure 2) and activity towards 8-oxo-dGTP is poor compared to that of the

human MTH1 enzyme. MTH1 is the primary sanitizer of oxidized nucleotides in humans and is over-expressed in numerous cancers.[14, 53] Inhibitors targeting human MTH1 provide a highly effective anti-cancer strategy, as the enzyme is essential for cancer cell survival, but is non-essential in normal cells.[14, 54] The low observed activity of AtNUDT1 with 8-oxo-dGTP suggests that AtNUDT1 has evolved to fulfill other roles in the cell apart from sanitizing the cell from oxidized nucleotides. Alternatively, the activity of AtNUDT1 may be regulated and increased by protein modifications and/or changes in cellular conditions.

Interestingly, AtNUDT1 has been shown to alter its substrate preference depending on the environmental concentration and species of metal ions.[6] In the presence of manganese chloride AtNUDT1 has low activity against NADH[23] whereas in the presence of magnesium, AtNUDT1 has activity against nucleotide substrates and DHNTP[20], which is involved in plant folate biosynthesis. However, at the normal physiological concentrations of metal ions present in plants, AtNUDT1 prefers magnesium for catalysis.[6] This feature may allow the enzyme to adapt to fluctuations of metal ions and substrates within the cell. It is possible that the enzyme is not as constrained to its role in oxidized nucleotide sanitization compared to *E. coli* MutT and human MTH1 as plants have developed other mechanisms that offer protection against ROS. These include anti-oxidative enzymes and large numbers of antioxidants such as tocopherol, ascorbate and glutathione.[55-57] The diversity of substrates for AtNUDT1 was further expanded by recent reports that AtNUDT1 is active against non-nucleotide monoterpene substrates.[24, 25]

Studies of *Rosa hybrid cultivar* Nudix1 (RhNUDT1) were the first to report that the plant Nudix enzymes can hydrolyze monoterpenes, a reaction previously shown to be carried out by monoterpene synthases.[58] Monoterpenes constitute up to 70 % of the scent compounds present in rose petals,[58] and thus their identification in *Arabidopsis* was somewhat unexpected due to the

general lack of scent in these plants.[59] No comparisons have been made between the levels of monoterpene scent compounds in roses and *Arabidopsis* to our knowledge. The largest numbers of monoterpene compounds produced by *A. thaliana* have been detected in floral tissues, which do not include flower petals. These volatiles, in addition to their roles in scent production, have other important cellular functions such as plant-plant interactions, communication with the surrounding environment, and the defense against pathogens.[26, 27] Interestingly RhNUDT1 was shown to have a low *K*m value (140 nM) for the monoterpene precursor GPP, but was shown to have extremely poor activity against 8-oxo-dGTP and dGTP.[58] The kinetic parameters of AtNUDT1 with the monoterpene substrates DMAPP, IPP, GPP and FPP were recently reported.[25] In that study AtNUDT1 did not display a dramatic preference for monoterpene substrates, with the catalytic efficiency of these reactions being only marginally better or the same as for 8-oxo-dGTP.[25]

Recently the structures of AtNUDT1 in complex with GPP[24] and IPP[28] were reported. The geranyl group of the GPP bound structure occupied two alternate conformations. One of these orientations was in a similar position to the base and deoxyribose moiety of 8-oxo-dGTP in our structure, whereas in the second, the geranyl group is directed towards a hydrophobic region of the binding pocket. Mutations of residues in this hydrophobic region reduced the activity of AtNUDT1 for GPP by up to 50 %.[24] These hydrophobic interactions may therefore play a role in the recognition of non-nucleotide substrates by AtNUDT1. The most striking difference between the GPP and 8-oxo-dGTP bound structures was the difference in the binding modes of the phosphate groups. Related Nudix enzymes have a conserved phosphate binding site, as evident in our comparisons of AtNUDT1 with human MTH1 and *E. coli* MutT. The AtNUDT1 GPP bound structure contains a mutation in one of the residues involved in the Nudix motif

(Glu56Ala) which completely abolishes enzyme activity.[24] This lack of activity can be explained by our 8-oxo-dGTP bound structure which shows that Glu56 contributes to the hydrogen bond network involved in coordinating the magnesium ions critical for the correct positioning and activation of the phosphate group. Extensive mechanistic studies of *E. coli* MutT have shown the enzyme requires two magnesium ions for activity.[60, 61] These divalent cations exhibit octahedral coordination involving conserved glutamate residues and a glycine from the conserved Nudix motif, the phosphate group of the substrate and additional water molecules.[62] Catalysis occurs by nucleophilic substitution by water at the internal the β-phosphate atom, generating the mononucleotide form of the substrate and pyrophosphate.[63] The reaction is accelerated by a glutamate residue form the Nudix motif which acts as a general base to activate the attacking water molecule.[64] The existing structures of MutT in the Protein Data Bank with its preferred substrate 8-oxo-dG are all the monophosphate product (8-oxo-dGMP). However, the proposed mechanism is supported by a solution NMR structure of MutT in complex with the non-hydrolysable analogue AMPCPP (PDB ID: 1TUM).[62, 65] The metal ions in the structure are critical for orienting the attacking catalytic water molecule, activating the phosphate group for nucleophilic attack and facilitating the departure of the anionic leaving group.[66] Mutations to the glutamate residues involved in magnesium coordination dramatically decreases the turnover of the enzyme,[24, 67] indicating that properly positioned metal ions contribute significantly to catalysis.

As the substrate has not been completely hydrolyzed in our structure, we can speculate regarding the catalytic mechanism of AtNUDT1. In 8-oxo-dGTP bound AtNUDT1 the two magnesium ions coordinate the oxygen atoms of the phosphate group, activating the β-phosphate for nucleophilic attack by an incoming water molecule. In addition, the residues His42 and

Lys110 are likely important for positioning the phosphate group as well as stabilizing the transition state. The interaction between Arg27 and the α-phosphate of the substrate may also enhance the departure of the nucleotide monophosphate (Supplementary Figure 3A). In our structure the water molecules in closest proximity to the β-phosphate of 8-oxo-dGTP are W180, W86 and W246 (Supplementary Figure 3A). However, it should be noted that all of these waters are positioned at least 3.7 Å from the β-phosphate atom. While W180 is positioned the closest out of these candidates (3.7 Å) it is not in the correct position for an in-line attack on the phosphate atom (Supplementary Figure 3A). The angle between W246, the β-phosphate and the leaving group is 160° degrees placing this water in an optimal position for an in-line attack.[66, 68] However, W246 is located at a distance of 5.3 Å from the β-phosphate, making it an unlikely candidate for the attacking nucleophile. W86 is likely a better candidate for the attacking water molecule. While the attack angle (138°) is less ideal than for W246, it is located significantly closer to the β-phosphate (4.0 Å) and coordinates with a magnesium ion (2.4 Å) also Glu60 (3.1 Å) and Glu107 (2.6 Å) either of which could potentially act as a base to activate W86 for nucleophilic attack (Supplementary Figure 3A). These comments are however speculative, and we cannot definitively claim from our structural data that it is in fact W86 which is the attacking nucleophile.

In IPP bound AtNUDT1 there is a water molecule at approximately the same position as W86 in our structure (Supplementary Figure 3B). This water molecule (W301) is 4.1 Å from the β-phosphate of the IPP substrate and coordinates with a magnesium ion (2.3 Å) and is in close enough proximity for activation by either Glu60 (2.7 Å) or Glu107 (2.3 Å)[28] (Supplementary Figure 3B). In addition, there is another water molecule (W392) in the IPP bound structure

which could be a candidate for the attacking nucleophile. W392 is 4.3 Å from the β-phosphate of the substrate and coordinates with a magnesium ion (2.8 Å). This magnesium ion in the IPP bound structure is located in the same position as the γ-phosphate in the 8-oxo-dGTP bound enzyme. The angle between W392, the β-phosphate and the leaving group is 170°, which more significantly more favorable for an in-line nucleophilic attack when compared to W301 (where the angle between the water, phosphate and leaving group is 133°). However, W392 is significantly further away from the residues Glu59 (4.1 Å) and Glu107 (4.2 Å) which would be required for activating the water molecule (Supplementary Figure 3B). Based on the available data it cannot be conclusively stated which of these water molecules carries out the hydrolysis reaction in the IPP bound structure.

The structures of AtNUDT1 bound with 8-oxo-dGTP and IPP are more likely to represent productive substrate binding modes compared to the GPP bound mutant enzyme. As noted previously, the Glu56Ala mutation would severely affect the coordination of the magnesium ions required for phosphate binding. In the IPP bound structure Glu56 actually coordinates two magnesium ions (rather than one in the 8-oxo-dGTP bound structure), both of which coordinate the β-phosphate of the substrate,[28] making this mutation particularly detrimental to metal coordination involving terpene substrates (Supplementary Figure 3). The Km value of 8 μM for monoterpenes[25] is likely closer to the cellular concentration of these compounds.[69] Km values of AtNUDT1 for 8-oxo-dGTP are around 30 μM, a lot higher than the cellular concentration of 8-oxo-dGTP.[70] As enzymes have usually evolved to have Km values for their substrates that are close to their actual cellular concentration,[71] this may suggest that the major role of AtNUDT1 is terpene metabolism. The significance of the diverse variety of substrates catalyzed by AtNUDT1 clearly requires further investigation. The AtNUDT1 of *Arabidopsis* has likely evolved to utilize

a broader range of substrates than its homologues from humans and bacteria, due to the specific environmental selection pressures and distinct cellular processes relevant to plants.

ASSOCIATED CONTENT

Supporting information

A. thaliana atnudt1 cDNA and AtNUDT1 protein sequences, comparison of 8-oxo-dGTP bound AtNUDT1 (PDB ID: 6FL4) with the AtNUDT1 apo structure (PDB ID: 6DBY), AtNUDT1 and hMTH1 activities against canonical and oxidized adenine and guanine nucleotides, hydrogen bond networks of 8-oxo-dGTP bound AtNUDT1 (PDB ID: 6FL4) and IPP bound AtNUDT1 (PDB ID: 6DBZ) indicating putative catalytic water molecules.

AUTHOR INFORMATION

Corresponding Authors

*Email: stenmark@dbb.su.se. Telephone: +46 8163729.

*Email: thomas.helleday@scilifelab.se. Telephone: +46762828907

Author Contributions

A.-S.J. and E.S. contributed equally to this work. P.S and T.H conceived the project and supervised the study. M.C. conducted the crystallization experiments. E.S. determined the structure presented in this paper, and analyzed the results. A.-S.J. performed site-directed mutagenesis, purified proteins, conducted biochemical experiments and analyzed data. E.S., A.-S.J., and P.S. analyzed data and wrote the manuscript. All authors reviewed the results, contributed to the writing, and approved the final version of the manuscript.

Funding Sources

This work was supported by the Swedish Research Council (T. Helleday, P. Stenmark), the Knut and Alice Wallenberg Foundation (T. Helleday, P. Stenmark), the Wenner-Gren Foundation (P. Stenmark), the Göran Gustafsson Foundation, the Swedish Children's Cancer Foundation, the Swedish Pain Relief Foundation, and the Torsten and Ragnar Söderberg Foundation (T. Helleday) and the Swedish Cancer Society (T. Helleday, P. Stenmark).

Notes

The authors declare no conflict of interest.

ACKNOWLEDGMENTS

We thank the beamline scientists at the European Synchrotron Radiation Facility (ESRF) for their support in structural biology data collection. We also thank PSF for protein production. We thank Kristina Edfeldt and Camilla Sjögren for administrative assistance and Sabina Eriksson and Flor Pineiro for lab management.

ABBREVIATIONS

MTH1, MutT homologue 1; PEG, polyethylene glycol; TCEP, tris(2-carboxyethyl)phosphine.

REFERENCES

[1] Bessman, M. J., Frick, D. N., and O'Handley, S. F. (1996) The MutT proteins or "Nudix" hydrolases, a family of versatile, widely distributed,"housecleaning" enzymes, *Journal of Biological Chemistry 271*, 25059-25062.

[2] Xu, W., Shen, J., Dunn, C. A., Desai, S., and Bessman, M. J. (2001) The Nudix hydrolases of Deinococcus radiodurans, *Molecular microbiology 39*, 286-290.

[3] Dunn, C. A., O'Handley, S. F., Frick, D. N., and Bessman, M. J. (1999) Studies on the ADP-ribose pyrophosphatase subfamily of the nudix hydrolases and tentative identification of trgB, a gene associated with tellurite resistance, *Journal of Biological Chemistry 274*, 32318-32324.

[4] McLennan, A. (2006) The Nudix hydrolase superfamily, *Cellular and Molecular Life Sciences CMLS 63*, 123-143.
[5] McLennan, A. G. (2013) Substrate ambiguity among the nudix hydrolases: biologically significant, evolutionary remnant, or both?, *Cellular and molecular life sciences 70*, 373-385.
[6] Kraszewska, E. (2008) The plant Nudix hydrolase family, *Acta Biochimica Polonica 55*, 663-671.
[7] Nakamura, T., Meshitsuka, S., Kitagawa, S., Abe, N., Yamada, J., Ishino, T., Nakano, H., Tsuzuki, T., Doi, T., and Kobayashi, Y. (2010) Structural and dynamic features of the MutT protein in the recognition of nucleotides with the mutagenic 8-oxoguanine base, *Journal of Biological Chemistry 285*, 444-452.
[8] Topal, M. D., and Baker, M. S. (1982) DNA precursor pool: a significant target for N-methyl-N-nitrosourea in C3H/10T1/2 clone 8 cells, *Proceedings of the National Academy of Sciences 79*, 2211-2215.
[9] Hayakawa, H., Hofer, A., Thelander, L., Kitajima, S., Cai, Y., Oshiro, S., Yakushiji, H., Nakabeppu, Y., Kuwano, M., and Sekiguchi, M. (1999) Metabolic fate of oxidized guanine ribonucleotides in mammalian cells, *Biochemistry 38*, 3610-3614.
[10] Haghdoost, S., Sjölander, L., Czene, S., and Harms-Ringdahl, M. (2006) The nucleotide pool is a significant target for oxidative stress, *Free Radical Biology and Medicine 41*, 620-626.
[11] Tajiri, T., Maki, H., and Sekiguchi, M. (1995) Functional cooperation of MutT, MutM and MutY proteins in preventing mutations caused by spontaneous oxidation of guanine nucleotide in Escherichia coli, *Mutation Research/DNA Repair 336*, 257-267.
[12] Maki, H., and Sekiguchi, M. (1992) MutT protein specifically hydrolyses a potent mutagenic substrate for DNA synthesis, *Nature 355*, 273.
[13] Svensson, L. M., Jemth, A.-S., Desroses, M., Loseva, O., Helleday, T., Högbom, M., and Stenmark, P. (2011) Crystal structure of human MTH1 and the 8‐oxo‐dGMP product complex, *FEBS letters 585*, 2617-2621.
[14] Gad, H., Koolmeister, T., Jemth, A.-S., Eshtad, S., Jacques, S. A., Ström, C. E., Svensson, L. M., Schultz, N., Lundbäck, T., and Einarsdottir, B. O. (2014) MTH1 inhibition eradicates cancer by preventing sanitation of the dNTP pool, *Nature 508*, 215.
[15] Carter, M., Jemth, A.-S., Hagenkort, A., Page, B. D., Gustafsson, R., Griese, J. J., Gad, H., Valerie, N. C., Desroses, M., and Boström, J. (2015) Crystal structure, biochemical and cellular activities demonstrate separate functions of MTH1 and MTH2, *Nature communications 6*, 7871.
[16] Foyer, C., Descourvieres, P., and Kunert, K. (1994) Protection against oxygen radicals: an important defence mechanism studied in transgenic plants, *Plant, Cell & Environment 17*, 507-523.
[17] Alscher, R. G., Donahue, J. L., and Cramer, C. L. (1997) Reactive oxygen species and antioxidants: relationships in green cells, *Physiologia Plantarum 100*, 224-233.
[18] Bowler, C., Montagu, M. v., and Inzé, D. (1992) Superoxide dismutase and stress tolerance, *Annual review of plant biology 43*, 83-116.
[19] Shigeoka, S., Ishikawa, T., Tamoi, M., Miyagawa, Y., Takeda, T., Yabuta, Y., and Yoshimura, K. (2002) Regulation and function of ascorbate peroxidase isoenzymes, *Journal of experimental botany 53*, 1305-1319.

[20] Klaus, S. M., Wegkamp, A., Sybesma, W., Hugenholtz, J., Gregory, J. F., and Hanson, A. D. (2005) A nudix enzyme removes pyrophosphate from dihydroneopterin triphosphate in the folate synthesis pathway of bacteria and plants, *Journal of Biological Chemistry 280*, 5274-5280.
[21] Ogawa, T., Ueda, Y., Yoshimura, K., and Shigeoka, S. (2005) Comprehensive analysis of cytosolic Nudix hydrolases in Arabidopsis thaliana, *Journal of Biological Chemistry*.
[22] Ogawa, T., Yoshimura, K., and Shigeoka, S. (2007) Functional analysis of an 8-oxo-7,8-dihydro-2 '-deoxyguanosine 5 '-triphosphate pyrophosphohydrolase, AtNUDX1, involved in repair of oxidative DNA damage in Arabidopsis thaliana, *Photosynth Res 91*, 284-285.
[23] Dobrzanska, M., Szurmak, B., Wyslouch-Cieszynska, A., and Kraszewska, E. (2002) Cloning and characterization of the first member of the Nudix family from Arabidopsis thaliana, *Journal of Biological Chemistry 277*, 50482-50486.
[24] Liu, J., Guan, Z., Liu, H., Qi, L., Zhang, D., Zou, T., and Yin, P. (2018) Structural Insights into the Substrate Recognition Mechanism of Arabidopsis GPP-Bound NUDX1 for Noncanonical Monoterpene Biosynthesis, *Molecular plant 11*, 218-221.
[25] Henry, L. K., Thomas, S. T., Widhalm, J. R., Lynch, J. H., Davis, T. C., Kessler, S. A., Bohlmann, J., Noel, J. P., and Dudareva, N. (2018) Contribution of isopentenyl phosphate to plant terpenoid metabolism, *Nature Plants 4*, 721-729.
[26] Pichersky, E., and Gershenzon, J. (2002) The formation and function of plant volatiles: perfumes for pollinator attraction and defense, *Current opinion in plant biology 5*, 237-243.
[27] Sun, P., Schuurink, R. C., Caissard, J.-C., Hugueney, P., and Baudino, S. (2016) My way: noncanonical biosynthesis pathways for plant volatiles, *Trends in plant science 21*, 884-894.
[28] Henry, L. K., Thomas, S. T., Widhalm, J. R., Lynch, J. H., Davis, T. C., Kessler, S. A., Bohlmann, J., Noel, J. P., and Dudareva, N. (2018) Contribution of isopentenyl phosphate to plant terpenoid metabolism, *Nature Plants 4*, 721-729.
[29] Li, X., Qiu, Y., Shen, Y., Ding, C., Liu, P., Zhou, J., and Ma, Z. (2008) Splicing together different regions of a gene by modified polymerase chain reaction-based site-directed mutagenesis, *Analytical biochemistry 373*, 398-400.
[30] Kabsch, W. (2010) Xds, *Acta Crystallographica Section D: Biological Crystallography 66*, 125-132.
[31] Winn, M. D., Ballard, C. C., Cowtan, K. D., Dodson, E. J., Emsley, P., Evans, P. R., Keegan, R. M., Krissinel, E. B., Leslie, A. G., and McCoy, A. (2011) Overview of the CCP4 suite and current developments, *Acta Crystallographica Section D 67*, 235-242.
[32] Vagin, A., and Teplyakov, A. (2010) Molecular replacement with MOLREP, *Acta Crystallographica Section D: Biological Crystallography 66*, 22-25.
[33] Matthews, B. W. (1968) Solvent content of protein crystals, *Journal of molecular biology 33*, 491-497.
[34] Langer, G., Cohen, S. X., Lamzin, V. S., and Perrakis, A. (2008) Automated macromolecular model building for X-ray crystallography using ARP/wARP version 7, *Nature protocols 3*, 1171.
[35] Emsley, P., and Cowtan, K. (2004) Coot: model-building tools for molecular graphics, *Acta Crystallogr D Biol Crystallogr 60*, 2126-2132.
[36] Murshudov, G. N., Vagin, A. A., and Dodson, E. J. (1997) Refinement of macromolecular structures by the maximum-likelihood method, *Acta Crystallogr D 53*, 240-255.

[37] Laskowski, R. A., Rullmann, J. A. C., MacArthur, M. W., Kaptein, R., and Thornton, J. M. (1996) AQUA and PROCHECK-NMR: Programs for checking the quality of protein structures solved by NMR, *J Biomol Nmr 8*, 477-486.
[38] Herold, N., Rudd, S. G., Ljungblad, L., Sanjiv, K., Myrberg, I. H., Paulin, C. B. J., Heshmati, Y., Hagenkort, A., Kutzner, J., Paget, B. D. G., Calderon-Montano, J. M., Loseva, O., Jemth, A. S., Bulli, L., Axelsson, H., Tesi, B., Valerie, N. C. K., Hoglund, A., Bladh, J., Wiita, E., Sundin, M., Uhlin, M., Rassidakis, G., Heyman, M., Tamm, K. P., Warpman-Berglund, U., Walfridsson, J., Lehmann, S., Grander, D., Lundback, T., Kogner, P., Henter, J. I., Helleday, T., and Schaller, T. (2017) Targeting SAMHD1 with the Vpx protein to improve cytarabine therapy for hematological malignancies, *Nat Med 23*, 256-263.
[39] Baykov, A. A., Evtushenko, O. A., and Avaeva, S. M. (1988) A Malachite Green Procedure for Ortho-Phosphate Determination and Its Use in Alkaline Phosphatase-Based Enzyme-Immunoassay, *Analytical Biochemistry 171*, 266-270.
[40] Holm, L., and Rosenstrom, P. (2010) Dali server: conservation mapping in 3D, *Nucleic Acids Res 38*, W545-W549.
[41] Krissinel, E., and Henrick, K. (2007) Inference of macromolecular assemblies from crystalline state, *Journal of Molecular Biology 372*, 774-797.
[42] Nissink, J. W. M., Bista, M., Breed, J., Carter, N., Embrey, K., Read, J., and Winter-Holt, J. J. (2016) MTH1 Substrate Recognition-An Example of Specific Promiscuity, *Plos One 11*.
[43] Waz, S., Nakamura, T., Hirata, K., Koga-Ogawa, Y., Chirifu, M., Arimori, T., Tamada, T., Ikemizu, S., Nakabeppu, Y., and Yamagata, Y. (2017) Structural and Kinetic Studies of the Human Nudix Hydrolase MTH1 Reveal the Mechanism for Its Broad Substrate Specificity, *Journal of Biological Chemistry 292*, 2785-2794.
[44] Bräutigam, L., Pudelko, L., Jemth, A.-S., Gad, H., Narwal, M., Gustafsson, R., Karsten, S., Puigvert, J. C., Homan, E., and Berndt, C. (2016) Hypoxic signaling and the cellular redox tumor environment determine sensitivity to MTH1 inhibition, *Cancer research*.
[45] Narwal, M., Jemth, A. S., Gustafsson, R., Almlof, I., Warpman Berglund, U., Helleday, T., and Stenmark, P. (2018) Crystal Structures and Inhibitor Interactions of Mouse and Dog MTH1 Reveal Species-Specific Differences in Affinity, *Biochemistry 57*, 593-603.
[46] Mishima, M., Sakai, Y., Itoh, N., Kamiya, H., Furuichi, M., Takahashi, M., Yamagata, Y., Iwai, S., Nakabeppu, Y., and Shirakawa, M. (2004) Structure of human MTH1, a nudix family hydrolase that selectively degrades oxidized purine nucleoside triphosphates, *Journal of Biological Chemistry 279*, 33806-33815.
[47] Bohlmann, J., and Keeling, C. I. (2008) Terpenoid biomaterials, *Plant J 54*, 656-669.
[48] Taddei, F., Hayakawa, H., Bouton, M. F., Cirinesi, A. M., Matic, I., Sekiguchi, M., and Radman, M. (1997) Counteraction by MutT protein of transcriptional errors caused by oxidative damage, *Science 278*, 128-130.
[49] Ito, R., Hayakawa, H., Sekiguchi, M., and Ishibashi, T. (2005) Multiple enzyme activities of Escherichia coli MutT protein for sanitization of DNA and RNA precursor pools, *Biochemistry 44*, 6670-6674.
[50] Venkateswarlu, D., and Leszczynski, J. (1998) Tautomerism and proton transfer in 6-selenoguanine: A post Hartree-Fock level ab initio SCF-MO investigation, *J Phys Chem A 102*, 6161-6166.

[51] Fujikawa, K., Kamiya, H., Yakushiji, H., Nakabeppu, Y., and Kasai, H. (2001) Human MTH1 protein hydrolyzes the oxidized ribonucleotide, 2-hydroxy-ATP, *Nucleic Acids Res 29*, 449-454.
[52] Sakai, Y., Furuichi, M., Takahashi, M., Mishima, M., Iwai, S., Shirakawa, M., and Nakabeppu, Y. (2002) A molecular basis for the selective recognition of 2-hydroxy-dATP and 8-oxo-dGTP by human MTH1, *Journal of Biological Chemistry 277*, 8579-8587.
[53] Kennedy, C. H., Pass, H. I., and Mitchell, J. B. (2003) Expression of human MutT homologue (hMTH1) protein in primary non-small-cell lung carcinomas and histologically normal surrounding tissue, *Free Radical Biology and Medicine 34*, 1447-1457.
[54] Berglund, U. W., Sanjiv, K., Gad, H., Kalderen, C., Koolmeister, T., Pham, T., Gokturk, C., Jafari, R., Maddalo, G., Seashore-Ludlow, B., Chernobrovkin, A., Manoilov, A., Pateras, I. S., Rasti, A., Jemth, A. S., Almlof, I., Loseva, O., Visnes, T., Einarsdottir, B. O., Gaugaz, F. Z., Saleh, A., Platzack, B., Wallner, O. A., Vallin, K. S. A., Henriksson, M., Wakchaure, P., Borhade, S., Herr, P., Kallberg, Y., Baranczewski, P., Homan, E. J., Wiita, E., Nagpal, V., Meijer, T., Schipper, N., Rudd, S. G., Brautigam, L., Lindqvist, A., Filppula, A., Lee, T. C., Artursson, P., Nilsson, J. A., Gorgoulis, V. G., Lehtio, J., Zubarev, R. A., Scobie, M., and Helleday, T. (2016) Validation and development of MTH1 inhibitors for treatment of cancer, *Ann Oncol 27*, 2275-2283.
[55] Mittler, R., Vanderauwera, S., Gollery, M., and Van Breusegem, F. (2004) Reactive oxygen gene network of plants, *Trends in Plant Science 9*, 490-498.
[56] Foyer, C. H., and Noctor, G. (2005) Oxidant and antioxidant signalling in plants: a re-evaluation of the concept of oxidative stress in a physiological context, *Plant Cell Environ 28*, 1056-1071.
[57] Wormuth, D., Heiber, I., Shaikali, J., Kandlbinder, A., Baier, M., and Dietz, K. J. (2007) Redox regulation and antioxidative defence in Arabidopsis leaves viewed from a systems biology perspective, *J Biotechnol 129*, 229-248.
[58] Magnard, J. L., Roccia, A., Caissard, J. C., Vergne, P., Sun, P. L., Hecquet, R., Dubois, A., Hibrand-Saint Oyant, L., Jullien, F., Nicole, F., Raymond, O., Huguet, S., Baltenweck, R., Meyer, S., Claudel, P., Jeauffre, J., Rohmer, M., Foucher, F., Hugueney, P., Bendahmane, M., and Baudino, S. (2015) Biosynthesis of monoterpene scent compounds in roses, *Science 349*, 81-83.
[59] Tholl, D., and Lee, S. (2011) Elucidating the Metabolism of Plant Terpene Volatiles: Alternative Tools for Engineering Plant Defenses?, *Recent Adv Phytochem 41*, 159-178.
[60] Frick, D. N., Weber, D. J., Gillespie, J. R., Bessman, M. J., and Mildvan, A. S. (1994) Dual divalent cation requirement of the MutT dGTPase. Kinetic and magnetic resonance studies of the metal and substrate complexes, *J Biol Chem 269*, 1794-1803.
[61] Harris, T. K., Wu, G., Massiah, M. A., and Mildvan, A. S. (2000) Mutational, kinetic, and NMR studies of the roles of conserved glutamate residues and of lysine-39 in the mechanism of the MutT pyrophosphohydrolase, *Biochemistry 39*, 1655-1674.
[62] Lin, J., Abeygunawardana, C., Frick, D. N., Bessman, M. J., and Mildvan, A. S. (1997) Solution structure of the quaternary MutT-M(2+)-AMPCPP-M(2+) complex and mechanism of its pyrophosphohydrolase action, *Biochemistry 36*, 1199-1211.

[63] Weber, D. J., Bhatnagar, S. K., Bullions, L. C., Bessman, M. J., and Mildvan, A. S. (1992) Nmr and Isotopic Exchange Studies of the Site of Bond-Cleavage in the Mutt Reaction, *Journal of Biological Chemistry 267*, 16939-16942.
[64] Abeygunawardana, C., Weber, D. J., Gittis, A. G., Frick, D. N., Lin, J., Miller, A. F., Bessman, M. J., and Mildvan, A. S. (1995) Solution Structure of the Mutt Enzyme, a Nucleoside Triphosphate Pyrophosphohydrolase, *Biochemistry 34*, 14997-15005.
[65] Mildvan, A. S., Weber, D. J., and Abeygunawardana, C. (1999) Solution structure and mechanism of the MutT pyrophosphohydrolase, *Adv Enzymol Ramb 73*, 183-+.
[66] Mildvan, A. S., Xia, Z., Azurmendi, H. F., Saraswat, V., Legler, P. M., Massiah, M. A., Gabelli, S. B., Bianchet, M. A., Kang, L. W., and Amzel, L. M. (2005) Structures and mechanisms of Nudix hydrolases, *Arch Biochem Biophys 433*, 129-143.
[67] Lin, J., Abeygunawardana, C., Frick, D. N., Bessman, M. J., and Mildvan, A. S. (1996) The role of Glu57 in the mechanism of the Escherichia coli MutT enzyme by mutagenesis and heteronuclear NMR, *Biochemistry 35*, 6715-6726.
[68] Strater, N. (2006) Ecto-5'-nucleotidase: Structure function relationships, *Purinergic Signal 2*, 343-350.
[69] Chen, F., Tholl, D., D'Auria, J. C., Farooq, A., Pichersky, E., and Gershenzon, J. (2003) Biosynthesis and emission of terpenoid volatiles from Arabidopsis flowers, *Plant Cell 15*, 481-494.
[70] Yoshimura, K., Ogawa, T., Ueda, Y., and Shigeoka, S. (2007) AtNUDX1, an 8-oxo-7,8-dihydro-2 '-deoxyguanosine 5 '-triphosphate pyrophosphohydrolase, is responsible for eliminating oxidized nucleotides in Arabidopsis, *Plant Cell Physiol 48*, 1438-1449.
[71] Bennett, B. D., Kimball, E. H., Gao, M., Osterhout, R., Van Dien, S. J., and Rabinowitz, J. D. (2009) Absolute metabolite concentrations and implied enzyme active site occupancy in Escherichia coli, *Nat Chem Biol 5*, 593-599.

TABLE OF CONTENTS GRAPHIC